Synthesis of quadruplex-forming tetra-end-linked oligonucleotides: Effects of the linker size on quadruplex topology and stability

ARTICLE *in* BIOPOLYMERS · JUNE 2009

Impact Factor: 2.39 · DOI: 10.1002/bip.21153 · Source: PubMed

8 AUTHORS, INCLUDING:

Nicola Borbone
University of Naples Federico II
102 PUBLICATIONS **701** CITATIONS
SEE PROFILE

Jussara Amato
University of Naples Federico II
74 PUBLICATIONS **358** CITATIONS
SEE PROFILE

Stefano d'errico
University of Naples Federico II
62 PUBLICATIONS **246** CITATIONS
SEE PROFILE

Michela Varra
University of Naples Federico II
44 PUBLICATIONS **274** CITATIONS
SEE PROFILE

Synthesis of Quadruplex-Forming Tetra-End-Linked Oligonucleotides: Effects of the Linker Size on Quadruplex Topology and Stability

Giorgia Oliviero, Nicola Borbone, Jussara Amato, Stefano D'Errico, Aldo Galeone, Gennaro Piccialli, Michela Varra, Luciano Mayol

Dipartimento di Chimica delle Sostanze Naturali, Università degli Studi di Napoli "Federico II," Via D. Montesano 49, I-80131 Napoli, Italy

Received 19 November 2008; revised 8 January 2009; accepted 20 January 2009
Published online 2 February 2009 in Wiley InterScience (www.interscience.wiley.com). DOI 10.1002/bip.21153

ABSTRACT:

*G-quadruplexes are characteristic structural arrangements of guanine-rich DNA sequences that abound in regions with relevant biological significance. These structures are highly polymorphic differing in the number and polarity of the strands, loop composition, and conformation. Furthermore, the cation species present in solution strongly influence the topology of the G-quadruplexes. Recently, we reported the synthesis and structural studies of new G-quadruplex forming oligodeoxynucleotides (ODNs) in which the 3′- and/or the 5′-ends of four ODN strands are linked together by a non-nucleotidic tetra-end-linker (TEL). These TEL-ODN analogs having the sequence TGGGGT are able to form parallel G-quadruplexes characterized by a remarkable high thermal stability. We report here an investigation about the influence of the reduction of the TEL size on the molecularity, topology, and stability of the resulting TEL-G-quadruplexes using a combination of circular dichroism (CD), CD melting, ^{1}H NMR spectroscopy, gel electrophoresis, and molecular modeling data. We found that all TEL-$(TGGGGT)_4$ analogs, regardless the TEL size and the structural orientation of the ODN branches, formed parallel TEL-G-quadruplexes. The molecular modeling studies appear to be consistent with the experimental CD and NMR data revealing that the G-quadruplexes formed by TEL-ODNs having the longer TEL (L**1**-**4**) are more stable than the corresponding G-quadruplexes having the shorter TEL (S**1**-**4**). The relative stability of S**1**-**4** was also reported. © 2009 Wiley Periodicals, Inc. Biopolymers 91: 466–477, 2009.*

Keywords: TEL-Quadruplex; solid-phase synthesis; circular dicroism; polyacrylamide gel electrophoresis

This article was originally published online as an accepted preprint. The "Published Online" date corresponds to the preprint version. You can request a copy of the preprint by emailing the Biopolymers editorial office at biopolymers@wiley.com

INTRODUCTION

G-quadruplexes are unique structures formed by Hoogsteen-type base pairing between four guanines and involving chelation of a metal ion. G-quadruplexes can be formed by intramolecular folding of guanine-rich sequences or by intermolecular association of two or four sequences leading to the formation of dimeric or tetrameric complexes.[1]

The biological importance of these structures is threefold: (1) the occurrence of short G-rich sequences able to fold into G-quadruplex structures at the ends of telomeric DNA in eukaryotic chromosomes,[2,3] (2) the high prevalence of G-rich sequences in a large number of eukaryotic and prokaryotic genomes, and the increasing number of G-quadruplexes arising from these sequences,[2,4,5] and (3) their presence in the scaffold of several aptamers that have the ability

Correspondence to: Gennaro Piccialli; e-mail: picciall@unina.it
Contract grant sponsor: Italian M.U.R.S.T. (P.R.I.N. 2007 and Progetto Integrato Oncologia)

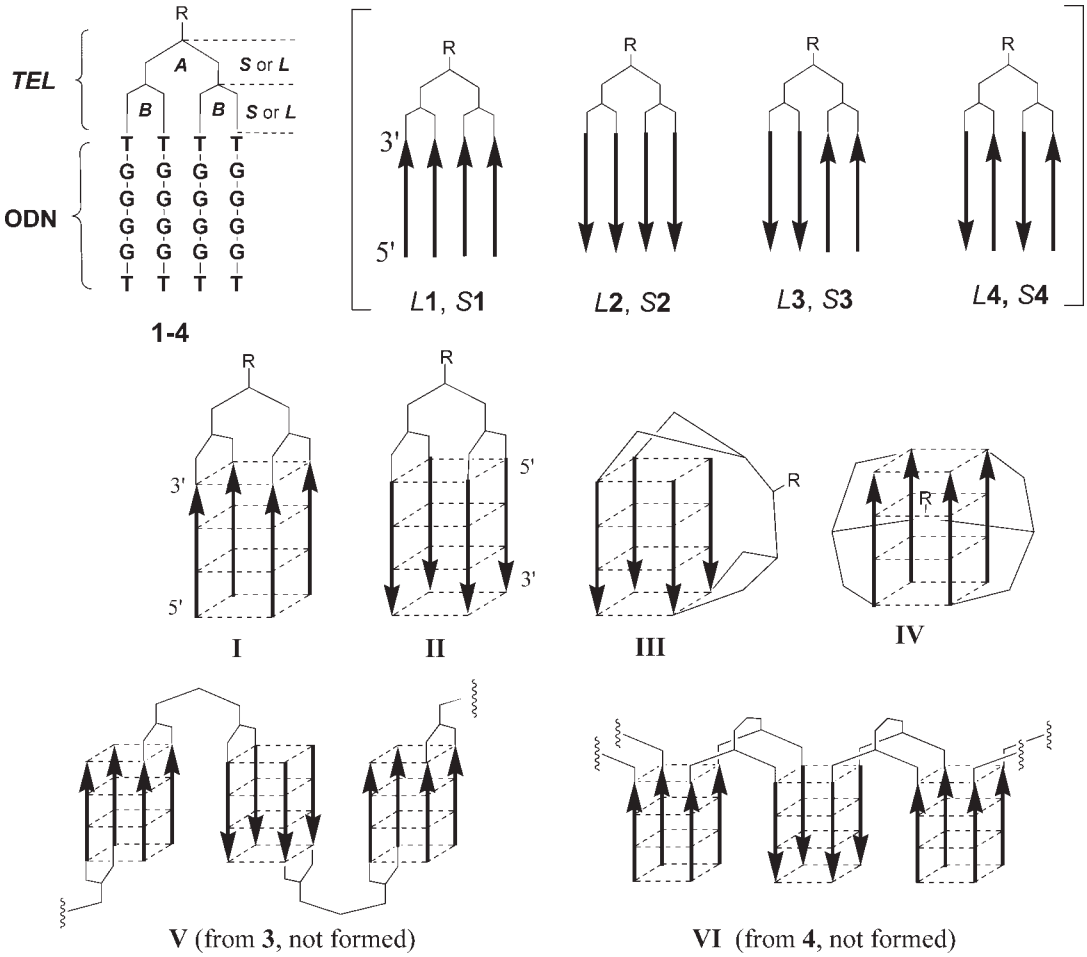

FIGURE 1 TEL ODNs **1**, **2**, **3**, and **4** and their structuration into G-quadruplex structures.

to selectively bind to biologically relevant proteins and small molecules.[6–10]

G-quadruplexes have the ability to form an array of conformations differing in structural features such as the molecularity, the relative orientation of the strands involved in the structure, the size of the loops connecting the strands, and the glycosidic conformation of guanosine residues (*syn* or *anti*).[11] The structural variability of G-quadruplexes further increases considering their capacity to accommodate A-, T-, and C-tetrads,[12–14] as well as tetrads formed by modified residues.[15,16] Finally, the topology and the chemical nature of the loops contribute to the structural variability of G-quadruplexes. Several studies have been devoted to the effects of the loops on G-quadruplex stability and structure.[17–20] Nucleotidic loops can lead to polymorphic G-quadruplex species whose structure depends on their length and base composition as well as on the nature of cation species present in solution.

We recently reported the synthesis of a new G-quadruplex forming oligodeoxynucleotide in which the 3′-ends of four ODN strands were linked together by a non-nucleotidic Tetra-End-Linker (TEL).[21] This TEL-ODN analog was able to form a parallel G-quadruplex provided with high thermal stability. These initial studies have been extended to other TEL-ODNs in which four d(TGGGGT) fragments were tethered to the TEL with different orientations[22] (**1**-**4**, Figure 1). The results indicated that all the synthesized TEL-ODNs **1**-**4** formed monomolecular parallel G-quadruplex structures (**I**-**IV**, Figure 1).

In this report, we have extended our previous studies to investigate the influence of the TEL size on the molecularity, topology, and stability of the G-quadruplex complexes resulting from TEL-ODNs. For this study, we have synthesized, by using the reported solid phase procedure, a new set of four TEL-d(TGGGGT)$_4$ ODNs (S**1**-**4**, Figure 1) in which the four ODN tracts are linked to one of the four branches of the new Short-TEL (S-TEL). The TEL-ODNs S**1**-**4** have been studied in comparison to the corresponding L**1**-**4** TEL-ODNs bearing the Long-TEL[22] (L-TEL).

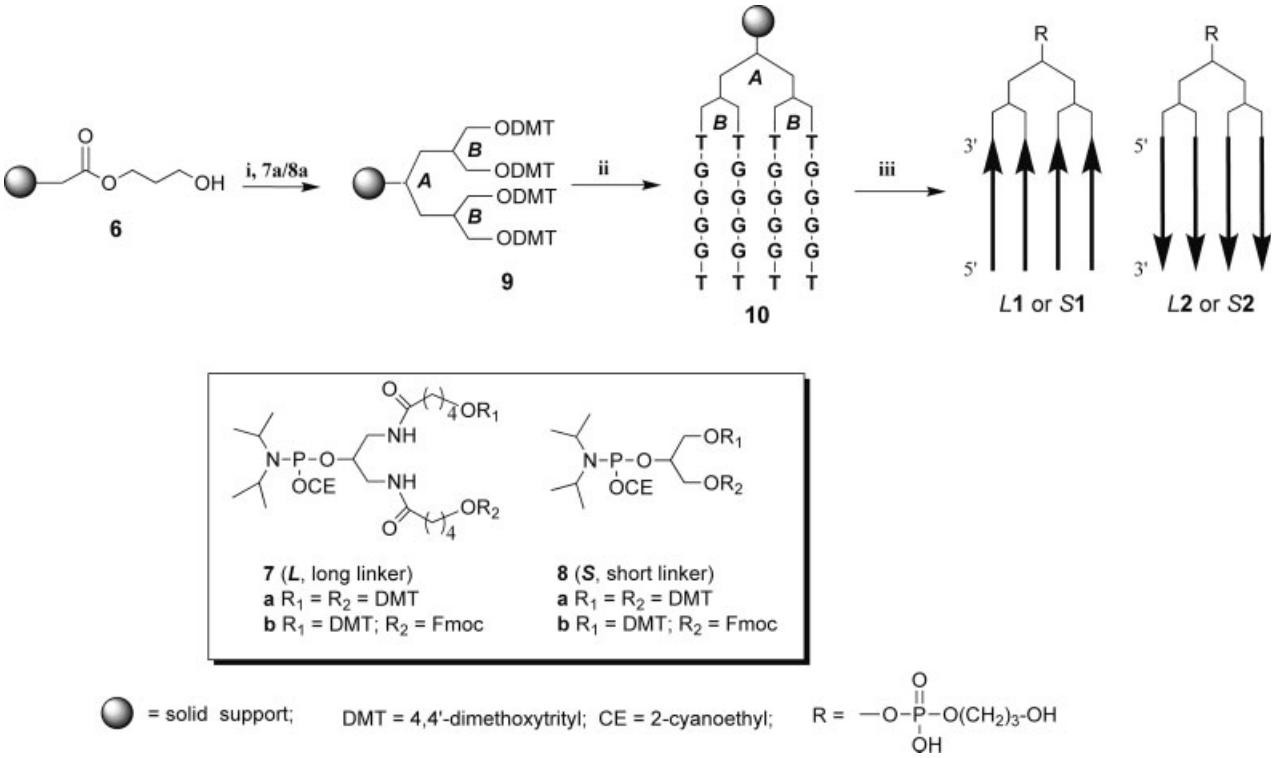

SCHEME 1 Synthetic procedure for TEL-ODNs L**1-2** and S**1-2**: (i) for L**1-2** two coupling cycles with **7a**, for S**1-2** two coupling cycles with **8a**; (ii) for TEL-ODNs **1** syntheses using 3′-phosphoramidite building blocks, for TEL-ODNs **2** syntheses using 5′-phosphoramidite building blocks; (iii) detachment from solid support and deprotection with conc. NH_4OH (7 h, 55°C).

RESULTS AND DISCUSSION

The S-TEL linker, like its progenitor, can be regarded as a single primary dibranched linker (**A** in **9**, Scheme 1) connected to two secondary dibranched linkers (**B** in **9**, Scheme 1). The shortening of the TEL linker has been achieved by embodying in **A** and **B** the *ad hoc* functionalized glycerol moieties whose synthetic phosphoramidite precursors **8a** and **8b** are shown in Scheme 1. Conversely, by using the long linker (**7a** or **7b**) in **A** and **B**, the L-TEL could be achieved. In the solid phase synthesis, the primary linker **A** allows the attachment of the ODN to the polymeric support, and the linkers **B** bear the 3′- or 5′-ends of the ODN tracts. The first synthetic pathway (Scheme 1) resulted in the synthesis of TEL-ODNs **1** and **2** in which the four ODN strands are parallel oriented and linked to the four TEL arms by their 3′- or 5′-ends, respectively. The second synthetic pathway (Scheme 2) leads to the synthesis of TEL-ODNs **3** and **4** each containing antiparallel oriented strands. Circular dichroism (CD), CD melting, ^{1}H NMR spectroscopy, molecular modeling and electrophoresis experiments have been used to explore the propensity of synthesized TEL-ODNs to fold into G-quadruplexes and to investigate their structures and stabilities.

Synthesis and Purification of TEL-ODNs type 1, 2, 3, and 4

For the synthesis of TEL-ODNs **1**, **2**, **3,** and **4,** we used a hydroxy-functionalized solid support **6** and the reactive bifunctional linkers **7** and **8**. In the first approach (Scheme 1), support **6**, by way of two coupling cycles with **7a** or **8a** performed on an automatic DNA synthesizer, yielded supports **9** bearing a symmetrical L- or S-TEL having the four primary alcohols protected by DMT groups. Supports **9** were then used to synthesize either L**1**, S**1** and L**2**, S**2** in which the four ODN strands are attached to the TEL via the 3′- or 5′-end. The reaction of 3′- or 5′-phosphoramidite nucleotide building blocks with **9** furnished the polymer bound TEL-ODNs **10** that after treatment with concentrated NH_4OH furnished L**1**, S**1** and L**2**, S**2**.

For the preparation of L**3** and S**3**, we adopted a synthetic strategy (Scheme 2) based on the use of linkers **7b** and **8b** in which the two alcoholic functions are orthogonally protected with Fmoc and DMT groups. Support **6**, by reaction with the phosphoramidite linker **7b** (or **8b**) yielded supports **11** that, after DMT deprotection and successive reaction with **7a** (or **8a**), furnished the tri-functionalized support **12**. Six coupling

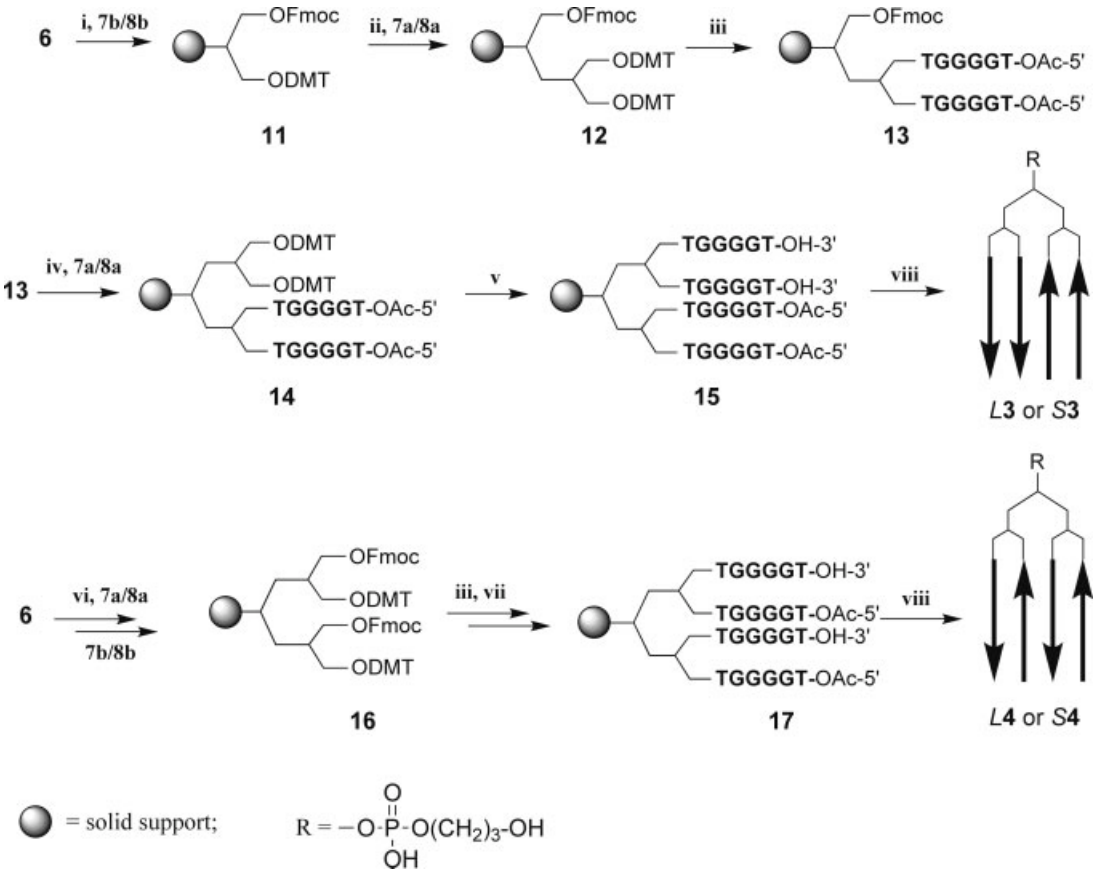

SCHEME 2 Synthetic procedure for TEL-ODNs L**3-4** and S**3-4**: (i) for L**3** coupling with linker **7b**, for S**3** coupling with linker **8b**; (ii) DMT removal and coupling with linker **7a** or **8a**, respectively, for L**3** or S**3**; (iii) DMT removal and ODN synthesis with 3′-phosphoramidites; (iv) Fmoc removal and coupling with appropriate linker **7a** or **8a**; (v) DMT removal and ODN synthesis with 5′-phosphoramidites; (vi) for L**4** a coupling cycle with **7a** and then **7b**, for S**4** a coupling cycle with **8a** and then **8b**; (vii) Fmoc removal and ODN synthesis with 5′-phosphoramidites; (viii) detachment from solid support and deprotection with conc. NH_4OH (7 h, 55°C).

cycles with 5′-phosphoramidite nucleotides and a final capping step of the 5′-OH ends, gave **13**. Removal of the Fmoc protecting group and coupling with **7a** (or **8a**) yielded the support **14** on which the second ODN domain was assembled using 5′-phosphoramidite nucleotides to obtain polymer bound TEL-ODNs **15**.

The synthetic pathway used to obtain TEL-ODNs L**4** and S**4** (Scheme 2), involved the reaction of **6** with **7a** (or **8a**) and subsequently with **7b** (or **8b**) to obtain the supports **16**. Removal of DMT protecting groups, followed by ODN synthesis with 5′-phosphoramidite nucleotides allowed the assembly of the first pair of ODN chains. After Fmoc deprotection, the remaining ODN pair having opposite polarity was then assembled using 5′-phosphoramidite nucleotides thus obtaining **17**. Detachment from the solid support and complete deprotection of type **3** and **4** TEL-ODNs were achieved by treating the supports **15** and **17**, respectively, with concentrated NH_4OH as described for **1** and **2**. Purification and analysis of crude products **1**, **2**, **3,** and **4** were carried out using HPLC. The ^1H NMR and MALDI-MS data confirmed the purity of the products. Purified samples of **1**, **2**, **3,** and **4** were dissolved in Na^+ and K^+ buffers and annealed to form G-quadruplexes.

CD and CD Thermal Analysis

To compare the propensity of each synthesized TEL-ODN to form a G-quadruplex structure, we carried out CD studies. CD spectra are used to assess the nature of G-quadruplex folding, though there is some debate about the CD signature of antiparallel and parallel G-quadruplexes. The vast majority of published reports are consistent with the observation that antiparallel G-quadruplexes display a maximum near 295 nm in the presence of sodium or potassium ions,

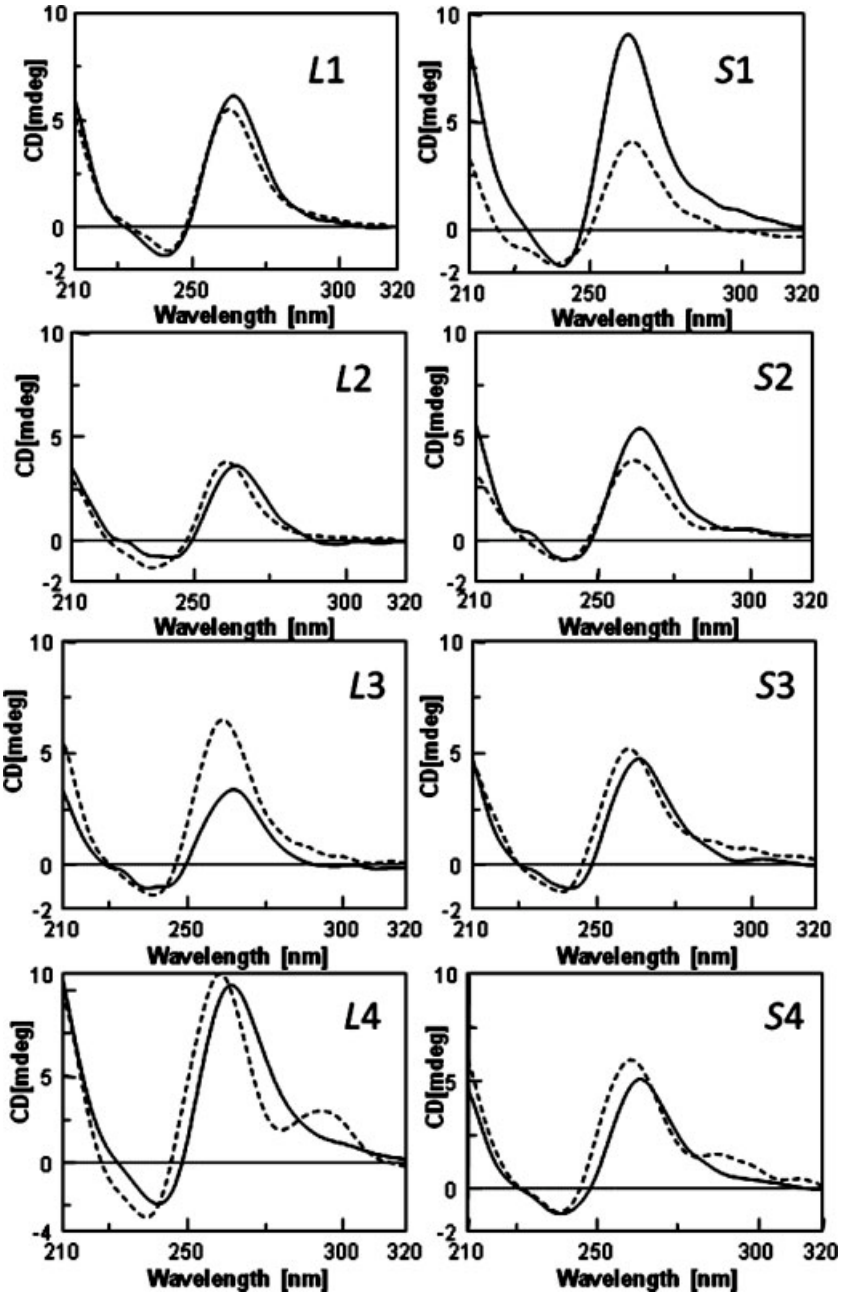

FIGURE 2 CD profiles of L**1**-**4** (left column) and S**1**-**4** (right column) in 80 m*M* Na^+ buffer (dotted line), and in 80 m*M* K^+ buffer (solid line) at 25°.

whereas parallel G-quadruplexes exhibit a maximum around 265 nm.[23–26] However, researchers must take into account that a growing number of exceptions to this rule are coming out.[27,28] The L**1**-**4** and S**1**-**4** samples, annealed at the concentration of 1.0×10^{-5} M, were analyzed by CD in 80 m*M* and 40 m*M* Na^+ (data not reported) and K^+ buffers at 25°C.

The CD spectra of all the samples, with the notably exceptions of L**4** and S**4**, exhibited very similar CD profiles regardless the nature of the cation and the medium ionic strength. In Figure 2 are reported the CD spectra in 80 m*M* Na^+ buffer, characterized by a maximum centered around 264 nm and a minimum centered around 244 nm, which are in agreement with the presence in solution of parallel stranded G-quadruplexes. In the case of L**4** and S**4**, the CD profiles showed two maxima centered at 264 nm (the higher) and 289 nm (the lower) thus indicating that a small amount of antiparallel G-quadruplex species could coexist in Na^+ buffer. These data suggest that all the TEL-ODNs **1** and **2**,

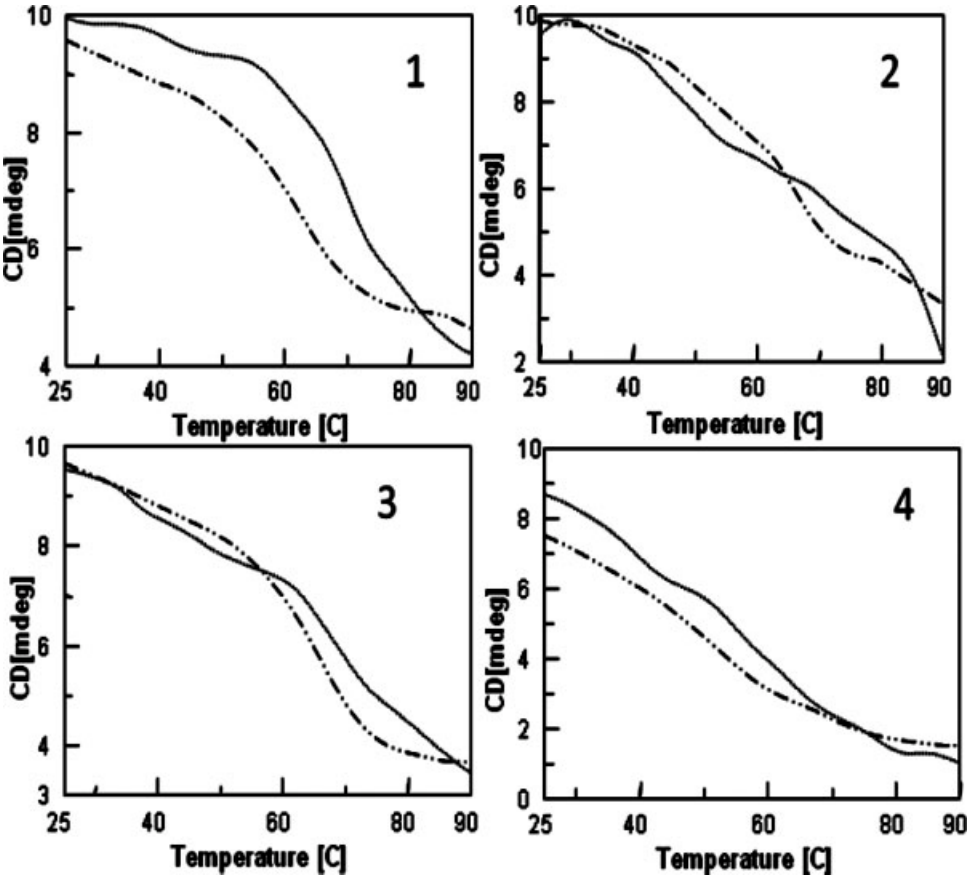

FIGURE 3 CD melting profiles at 264 nm (25–90°C, 0.5°C/min) of L**1**-**4** (dotted line) and S**1**-**4** (solid line) in 40 m*M* Na^+ buffer.

irrespectively of the TEL size, fold into parallel G-quadruplexes (types **I** and **II**, respectively, Figure 1) when annealed in Na^+ or K^+ buffers, indicating that the shortening of the TEL is compatible with the formation of parallel G-quadruplex structures.

For TEL-ODNs **3** and **4**, both embodying antiparallel ODN strands, the CD spectra disclosed the formation of parallel G-quadruplexes even in the presence of the S-TEL. Furthermore, it is to be noted that the replacement of the L-TEL with the S-TEL did not modify the intensity ratio between the two CD maxima observed in the CD spectra of L**4** and S**4** in Na^+ buffer at 25°C. As suggested in our previous report,[22] the CD spectra recorded for ODNs type **3** and **4** are coherent with the formation of type **III** and **IV** monomolecular parallel G-quadruplexes.

To evaluate the influence of TEL size on the stability of the resulting TEL-quadruplexes, CD thermal denaturation experiments were performed in 80 m*M* and 40 m*M* Na^+ and K^+ buffers. The CD value (mdeg) at 264 nm was monitored in the range 25–90°C at a heating rate of 0.5°C/min. Because within the temperature range examined low or irrelevant mdeg variation were observed in 80 m*M* Na^+ and K^+ buffers, the here reported data are limited to the thermal denaturation studies recorded in 40 m*M* Na^+ buffer (see Figure 3). The melting curves of L**1**-**4** display a significant decrease of mdeg values because the beginning of the analyses. This response, especially for L**2** and L**4**, induces a not negligible error in the determination of T_m values, and it could suggest the coexistence in solution of several kinds of structures that melt at different temperatures. Notwithstanding, well defined sigmoidal melting curves are observed for L**1** and L**3** allowing the calculation of their T_m (62 and 64°C, respectively). Marked multiphasic profiles are observed in the melting curves of S**1**-**4**, thus preventing the T_m determination of the resulting G-quadruplexes. Furthermore, the melting profiles of S**1**-**3** indicate that the melting process of these TEL-ODNs is not completed even at 90°C.

Native Gel Electrophoresis

We carried out nondenaturing PAGE experiments to investigate the electrophoretic behavior of the L**1**-**4** (Figure 4A) and

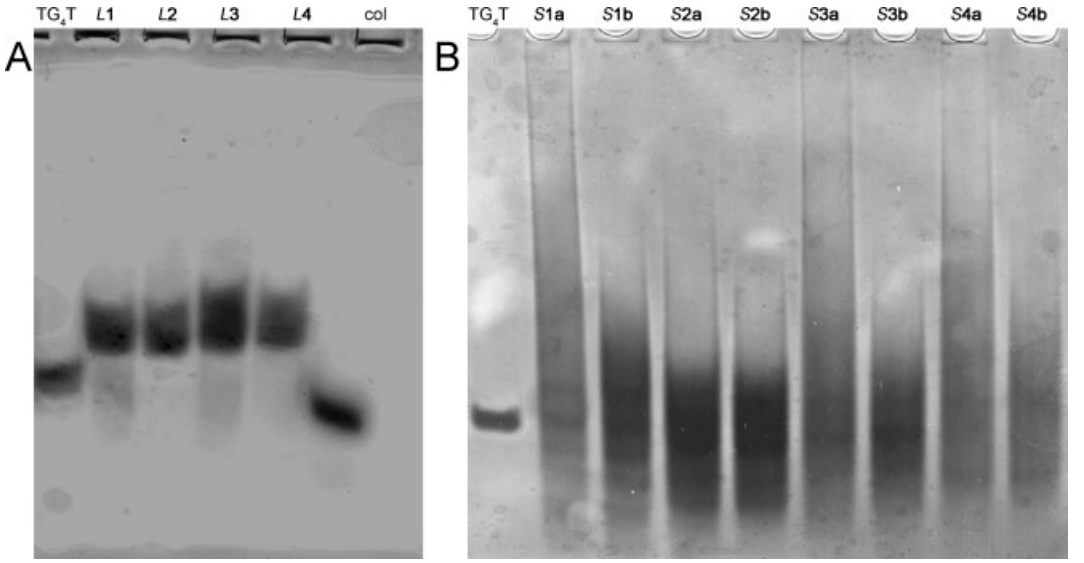

FIGURE 4 Nondenaturing 20% PAGE (pH 7.0): L**1**-**4** (PAGE *A*) annealed at 400 μM TEL-ODN concentration in 80 m*M* Na^+ buffer, col = Stains-All (Sigma); S**1**-**4** (PAGE *B*) annealed at 400 μM TEL-ODN concentration (lanes S**1a**-S**4a**), and annealed at 10 μM TEL-ODN concentration (lanes S**1b**-S**4b**) in 80 m*M* Na^+ buffer.

S**1**-**4** samples (Figure 4B), both annealed in 80 m*M* Na^+ buffer.

We observed that L**1**-**4**, annealed at 400 μM TEL-ODN concentration, showed prevalently a defined band with a mobility comparable to that of the tetramolecular $(TGGGGT)_4$. These bands, which we hypothesize corresponding to the intramolecular G-quadruplexes (**I**, **II**, **III** and **IV**, Figure 1), were not present in all S**1**-**4**, for which a marked slow smear was observable (Figure 4B). Similar migration profiles were observed in 80 m*M* K^+ buffer (data not shown). PAGE experiments performed in 40 m*M* of Na^+ gave substantially the same results. A different annealing condition was examined for the S**1**-**4** TEL-ODNs to investigate the effect of TEL-ODN concentration on the smear. In the PAGE reported in Figure 4B, the lanes **a** and **b** contain S**1**-**4** annealed at 400 μM and 10 μM TEL-ODN concentrations, respectively. We observed that the 10 μM TEL-ODN diluted annealing condition leads to a reduction of the smear which could be attributed to the formation of amorphous aggregates that dissociate during the PAGE run. This hypothesis is corroborated by the CD melting data that show in the case of S**1**-**4** analogues a multiphasic profile that could be attributed to the melting of the aggregates as described earlier.

^{1}H NMR Studies on L- and S-TEL-ODNs

^{1}H NMR studies at 25, 45, 65, and 85°C on L- and S-TEL-ODN samples **1**, **2**, **3**, and **4** were performed at 0.5 m*M* quadruplex concentration in H_2O/D_2O (9:1, v/v) in 10 m*M* KH_2PO_4, 0.2 m*M* EDTA and 70 m*M* KCl, pH 7.0. All spectra recorded at 25°C (see Figure 5) show the presence of broad signals in the range 10.9–11.8 ppm attributable to the exchange protected imino protons involved in Hoogsteen N(1)/O(6) hydrogen bonds of G-quartets.[29,30] In all cases, an increase in the temperature resulted in the sharpening of all imino proton signals. This phenomenon could be tentatively explained by the presence in solution of aggregates of monomolecular G-quadruplexes, which melt at temperatures above 25°C. In the case of L**1**-**3** and S**1**, the aggregates are almost completely melted at 45°C. In fact at this temperature four well resolved signals are detected in the imino proton region. No further sharpening of imino proton signals was observed at 65 and 85°C.

The ^{1}H NMR spectra of S**2** and S**3** show broader imino proton signals at 25°C than those observed for L**1**-**3** and S**1** that progressively sharpen when the temperature is increased from 25 to 65°C. For S**3**, the imino proton signals are significantly attenuated at 85°C with a complete loss of the signal at 11.6 ppm at this temperature. These data suggest that S**3** folds into a less stable G-quadruplex when compared with those formed by L**1**-**3** and S**1** and that more stable and/or extended aggregates may be present in solution. The imino proton regions for L**4** and S**4** are almost superimposable at 25°C. Very broad, overlapped signals are observed at 25°C that progressively sharpen as the temperature is increased to 85°C. At this temperature, four G-tetrad signals are still

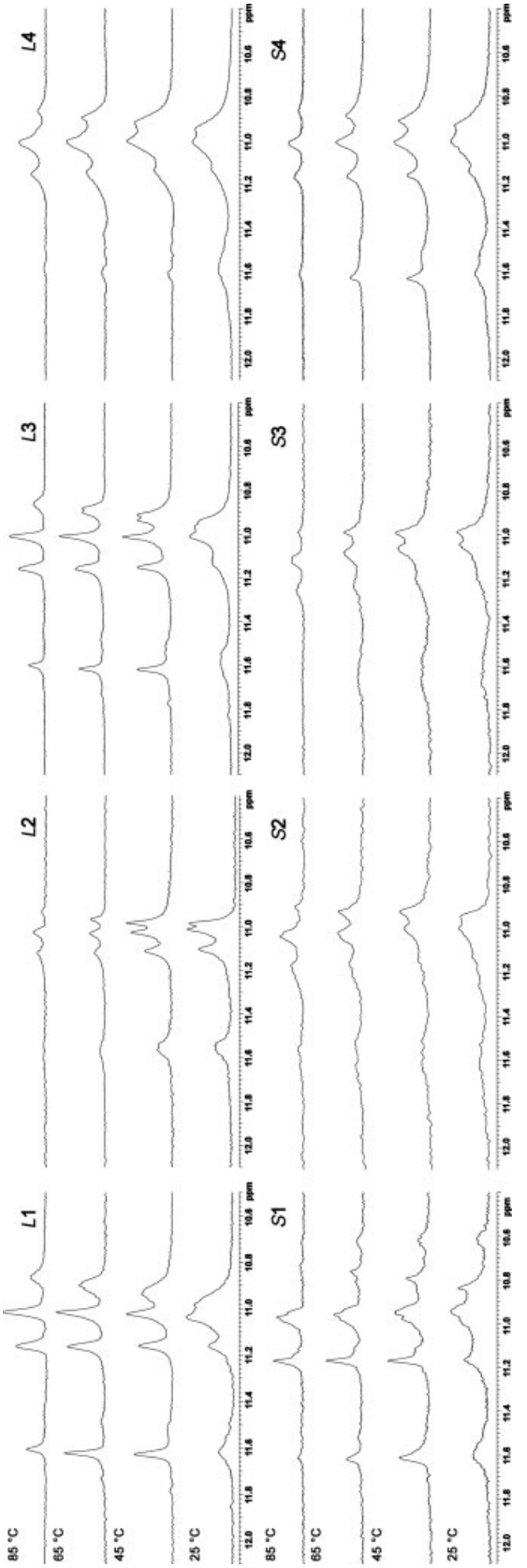

FIGURE 5 Imino proton regions of 500-MHz ^{1}H NMR spectra of L**1**-**4** and S**1**-**4** in 80 m*M* K^+ buffer.

clearly visible for S**4**, whereas the signal at 11.6 ppm is almost completely undetectable for L**4**. The NMR data indicate that all L- and S-TEL-ODN analogs fold into a G-quadruplex structure when annealed in K^+ buffer. Furthermore, the data suggest that all analogs fold into very similar parallel G-quadruplex structures (presumably monomolecular) at 65 and 85°C because at these temperatures all the imino proton signals occur at about the same chemical shift. TEL-ODN S**2**-**4** seem to favour the formation of more extended/stable aggregates. The ^{1}H NMR spectra in Na^+ buffer (data not shown) suggested the formation of G-quadruplex structures with lower thermal stability as well as the presence in solution of aggregates at lower temperatures for each of the S TEL-ODN analogs.

Molecular Modeling

Molecular modeling was used to investigate the propensity of TEL-ODNs assembled with the short TEL (S**1**-**4**) to adopt parallel G-quadruplex structures. The energy minimized structures obtained are shown in Figure 6. Inspection of the minimized structure of S**1** and S**2** reveals that, despite its shorter length, the S-TEL is still able to connect the four 3′- or 5′- ends of the strands, respectively, without causing any distortion in the overall G-quadruplex structure. Specifically, the integrity of G-tetrad stacking and Hoogsten hydrogen bonding interactions are maintained after energy minimization. In the case of S**3** and, to a greater extent, S**4**, the models clearly show that the linkers are too short to span the distance between the linked 5′- and 3′-ends of the strands assembled in a parallel G-quadruplex structure, requiring the involvement of the four thymidines directly linked to the TEL to function as an extended linker. Although the overall integrity of the G-tetrads core is maintained after energy minimization for S**3** and S**4**, a detailed analysis of the nature of the H-bonding within the G-tetrads reveals some important differences. Specifically, while optimum distances and angles between H-bond donor and acceptor atoms are observed in the case of S**3**, significant deviations are observed for S**4** resulting in less stable hydrogen bonding between the G residues of each tetrad so that only two or three hydrogen bonds in each G-tetrad are retained in the minimized G-quadruplex structure.

The molecular modeling studies appear to be consistent with the experimental CD and NMR data revealing that the G-quadruplexes formed by L**1**-**4** are more stable than the corresponding originated by S**1**-**4**. On the basis of molecular modeling data the relative stability of S**1**-**4** G-quadruplexes follows the order S1 $\cong$ S2 $>$ S3 $>$ S4.

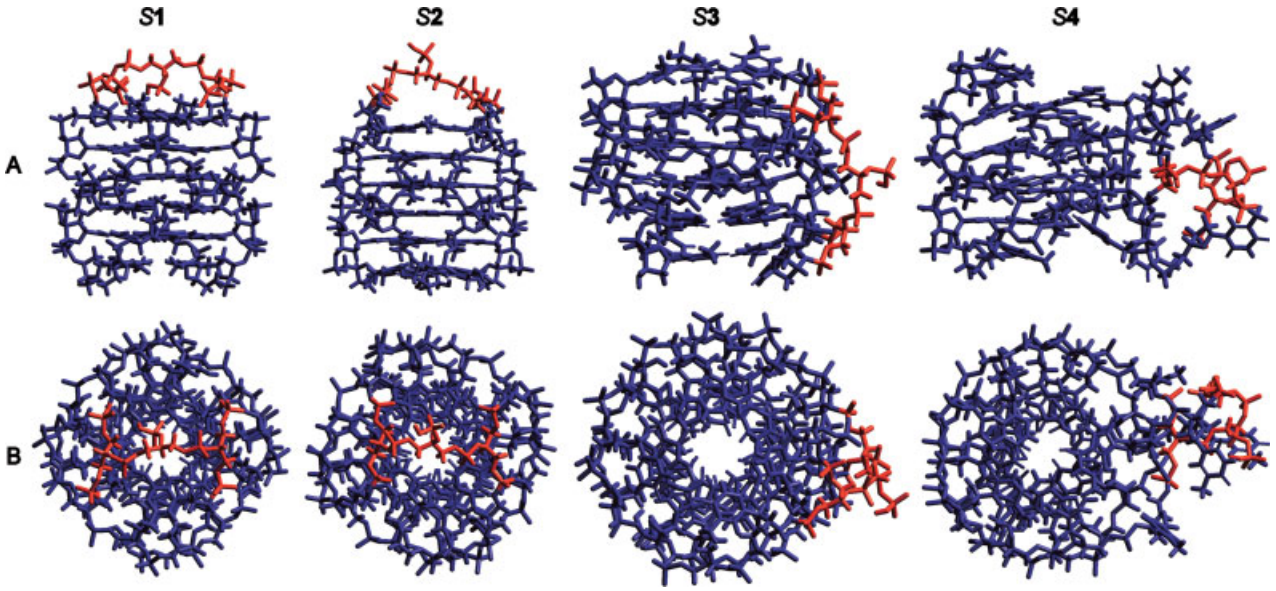

FIGURE 6 Molecular model pictures of G-quadruplex structures S**1**-**4**; A: front view; B: top view. The Tetra-End-Linker is in red.

CONCLUSIONS

In this article, we have investigated the G-quadruplex structures formed by several TEL-d(TGGGGT)$_4$ analogs differing for both the relative orientation of the four ODN strands attached to the non-nucleotidic TEL and the TEL size. The molecularity, topology, and stability of the resulting TEL-G-quadruplexes have been investigated using a combination of methods. CD spectra indicate that all TEL-ODN analogs, independently from the TEL size and the structural orientation of the ODN strands, formed parallel TEL-G-quadruplexes. Molecular modeling results point out the ability of the S-TEL to fold around the G-quadruplex scaffold, thus allowing the formation of monomolecular G-quadruplexes such as **I**-**IV** depicted in Figure 1. ^{1}H NMR studies confirmed the folding into parallel G-quadruplexes for all the here reported TEL-ODN species. Furthermore, the nondenaturing PAGE experiments of S**1**-**4** showed significant smearing with no single well defined G-quadruplex band. We attributed the significant smearing observed in PAGE experiments to the formation of aggregates made of single G-quadruplex scaffolds, which melt at low temperature and are not detectable by the MS technique. This hypothesis was also corroborated by the ^{1}H NMR analyses at increasing temperature, although the coexistence of TEL-ODN self-assembly phenomena cannot be excluded. The role of the TEL size seems to be crucial in the formation of these aggregates because they were observed almost exclusively for the S-TEL-ODNs. Although, from a theoretical point of view, TEL-ODNs could be able to form polymeric species like **V** and **VI** (see Figure 1), we rule out this hypothesis on the basis of the following considerations: (i) polymeric species like **V** and **VI** should be stable enough to allow a straightforward observation by the standard techniques used for quadruplex structural studies, (ii) no polymeric species have been detected in the MALDI mass spectra, and (iii) no defined bands attributable to dimeric or polymeric species have been detected during the PAGE experiments.

In conclusion, we have characterized a small set of parallel TEL-G-quadruplexes whose parallel topology was independent of the nature of the cation species in solution and of the TEL size. Furthermore, the invariable parallel orientation of the G-quadruplex structures leads to a predictable TEL loop arrangement on either the 5′-face, the 3′-face or on one side of the G-quadruplex scaffold. These findings, together with the ability to affect the stability of the TEL-G-quadruplexes through modification of the TEL, indicate that the TEL-ODNs are useful models to study ligand-quadruplex interactions. Furthermore, we believe that TEL-G-quadruplexes with suitable sequences could be used as new kind of aptamers, decoys, and molecular probes.

MATERIALS AND METHODS

Reagents and Equipment

Chemicals and solvents were purchased from Fluka-Sigma-Aldrich. Reagents and phosphoramidites for DNA syntheses were purchased from Glen Research. HPLC analyses and purifications were per-

formed with a JASCO PU2089 pump system equipped with an UV detector model 2075 Plus using a Merck Hibar (5 μm, 250–10) column. The linkers **7a-b** were purchased from Glen Research. Tentagel carboxy resin, used as starting material for preparation of solid support **6**, was purchased from Novabiochem. Preparation of **6** was carried out in a short column (10 cm length, 1 cm i.d.) equipped with a sintered glass filter, a stopcock, and a cap as described earlier.[22] The ODNs were assembled by a PerSeptive Biosystems Expedite DNA synthesizer using phosphoramidite chemistry. UV spectra were collected using a Jasco V-530 spectrophotometer. CD spectra and thermal denaturation experiments were collected with a Jasco J-715 spectropolarimeter equipped with a JASCO ETC-505T temperature controller unit, using a 0.1 cm path length quartz cuvette. ^{1}H NMR data were collected on Unity INOVA 500 and Mercury VX 400 Varian spectrometers equipped with a broadband inverse probe with *z*-field gradient, and processed using the Varian VNMR software package. MALDI-TOF mass spectrometric analyses were performed on a Bruker Autoflex mass spectrometer using a picolinic/3-hydroxy-picolinic acid mixture as the matrix. ESI-MS were performed on an Applied Biosystem API 2000 mass spectrometer. The ODN concentration was determined spectrophotometrically at λ = 260 nm and 90°C, using the molar extinction coefficient ε = 57,800 cm^{-1} M^{-1} calculated for the unstacked oligonucleotide by the nearest neighbor mode.[31]

Syntheses of Linkers 8a-b

8a: 0.34 g (3.6 mmol) of 1,2,3-propanetriol dried by repeated coevaporations with anhydrous pyridine and then dissolved in 8 mL of the same solvent, were reacted with 2.5 g (7.2 mmol) of 4,4′-dimethoxytrytilchloride at R.T. for 12 h. The reaction was quenched by addition of water and the resulting mixture, taken to dryness and redissolved in benzene, was purified on a silica gel column giving 1.63 g (2.34 mmol, 65% yield) of 1,3-bis-(O-DMT)-propanetriol, in mixture with the full protected derivative. The bis-tritylated compound was dissolved in dry CH_2Cl_2 (5 mL) and *N*,*N*-diisopropylethylamine was added (0.860 mL, 4.6 mmol) followed by 2-cyanoethyl-*N*,*N*-diisopropylchlorophosphoramidite (0.48 mL, 2.76 mmol). The mixture was stirred for 1 h at R.T. then diluted with ethyl acetate (50 mL) and washed with saturated sodium chloride solution (4 × 25 mL). The organic phase was dried over sodium sulphate and evaporated to an oil in the presence of toluene (10 mL). The product was purified by short column chromatography on Kieselgel 60H (10 g) eluting with CH_2Cl_2/ethyl acetate/2,6-lutidine 50:50:2 (v/v/v). The product was dried to give a white powder (90% yield). ^{1}H NMR (400 MHz) ppm (acetone, d6) 1.05 (d, 12H, $CHCH_3$), 2.97 (m, 2H, $CHCH_3$), 3.52 (d, 4H, CH_2ODMT), 3.82 (s, 12H, OCH_3), 3.87 (m, 1H, CHOP), 4.05 (s, 2H, CH_2CN), 6.82–7.55 (m, 26H, aromatic protons). ESI-MS calculated for $C_{53}H_{59}N_2O_8P$ *m/z*: 882.40, found: 883.40 $(M + H)^+$.

8b: 0.34 g (3.6 mmol) of 1,2,3-propanetriol dissolved in 8 mL of pyridine were reacted with 0.325 g (0.9 mmol) of 4,4′-dimethoxytrytilchloride at R.T. for 12h to afford after purification the monotrityl derivative as the main product (0.343 g, 0.8 mmol, 80% yield). This latter was protected at the remaining primary hydroxyl group by the reaction with fluorenylmethoxycarbonylchloride (Fmoc-Cl 232 mg, 0.9 eq) in anhydrous CH_2Cl_2. Phosphoramidite derivative was prepared as just described for obtaining **8a**. ^{1}H NMR (400 MHz) ppm (acetone, d6): 1.05 (d, 12H, $CHCH_3$), 2.97 (m, 2H, $CHCH_3$), 3.52 (d, 2H, CH_2ODMT), 3.82 (s, 6H, $4OCH_3$), 4.05 (s, 2H, CH_2CN), 4.14 (m, 1H, CHOP), 4.31(d, 2H, CH_2OFmoc), 4.46 (t, 1H, CH-fluorenyl), 4.78 (d, 2H, CH_2-fluorenyl), 6.80-7.65 (m, 21H, aromatic protons). ESI-MS calculated for $C_{47}H_{51}N_2O_8P$ *m/z*: 802.34, found: 803.80 $(M + H)^+$.

Syntheses and Purifications of TEL-ODNs L1-2 and S1-2

50 mg of support **6** (0.18 meq/g) were used for each synthesis in the automated DNA synthesizer following standard phosphoramidite chemistry, using 45 mg/mL of solution of phosphoramidite **7a** in two coupling cycles for the synthesis of L**1**, or using **8a** (two coupling cycles) for the synthesis of S**1** followed by reaction with 3′-phosphoramidite (for L**1** and S**1**) or 5′-phosphoramidite (for L**2** and S**2**) nucleotide building blocks (six cycles, 45 mg/mL in anhydrous CH_3CN) to obtain the polymer bound ODN **10**. The coupling yields were consistently higher than 98% (by DMT spectrophotometric measurements). The solid support **10** was then treated with conc. aq. ammonia solution for 7 h at 55°C. The filtered solution and washings were concentrated under reduced pressure and purified by HPLC on a Nucleogel SAX column eluted with a linear gradient of the following buffers. Buffer A: 20 m*M* NaH_2PO_4, pH 7.0 containing 20% CH_3CN; buffer B: 1*M* NaCl, 20 m*M* NaH_2PO_4, pH 7.0, containing 20% CH_3CN; linear gradient from 0 to 100% B in 30 min, flow rate 1 mL/min. The collected products were desalted by gel filtration on a Sephadex G25 column eluted with H_2O/ethanol (9:1,v/v) to obtain, after lyophilization, pure L**1**, L**2**, S**1,** and S**2** (82, 80, 74, and 76 OD_{260} units, respectively). The TEL-ODNs were characterized by MALDI TOF-MS (negative mode): L**1** found: 8814 (calcd. 8815.7); L**2** found: 8814 (calcd. 8815.7); S**1** found: 8220 (calcd. 8220.9); S**2** found: 8220 (calcd. 8220.9).

Syntheses and Purifications of TEL-ODNs 3 and 4

For the synthesis of L**3** and S*3*, 50 mg of support **6** (0.18 meq/g) was reacted, in the automated DNA synthesizer, with **7b** (for L**3**) or **8b** (for S**3**) following the standard phosphoramidite chemistry yielding support **11** (0.17 meq/g of DMT groups). After removal of DMT protecting groups by DCA, the second coupling cycle was performed in the same manner using phosphoramidite **7a** (for L**3**) or **8a** (for S**3**) thus obtaining support **12** (0.30 meq/g of DMT groups). **12** was then subjected to six coupling cycles using 3′-phosphoramidite nucleotide building blocks (45 mg/mL in CH_3CN), followed by final DMT removal and 5′-OH capping with Ac_2O, to yield ODN functionalized support **13**. The removal of Fmoc groups was achieved by treatment with piperidine/DMF solution (2:8, v/v, 30 min R.T.). The resulting support was then reacted with phosphoramidite **7a** or **8a** as described earlier thus obtaining **14** (0.27 meq/g of DMT groups). After removal of DMT protecting groups, the second ODN domain was assembled by six coupling cycles with 5′-phosphoroamidite nucleotide building block as described for support **12** yielding the polymer bound ODN **15**.

For the synthesis of L**4** and S**4**, support **6** (50 mg) was functionalized with appropriate **7a** or **8a** and then **7b** or **8b**, as described earlier, yielding the tetra-branched support **16** (0.28 meq/g of DMT groups). After removal of the DMT protecting groups, the first two ODN chains were assembled, using 3′-phosphoramidite nucleotide building blocks. After capping of the terminal 5′-OH functions by

Ac_2O treatment, the Fmoc groups were removed as previously described, and two successive ODN chains were assembled using 5′-phosphoroamidite nucleotide building blocks, thus obtaining the polymer bound ODN **17**. TEL-ODNs were detached from the supports **15** and **17**, deprotected and purified as described earlier. After lyophilization, the final pure products L**3,** S**3**, L**4,** and S**4** (65, 72, 69, and 80 OD_{260} units, respectively) were characterized by MALDI TOF-MS (negative mode): L**3** found: 8814 (calcd. 8815.7); L**4** found: 8815 (calcd. 8815.7); S**3** found: 8219 (calcd. 8220.9); S**4** found: 8220 (calcd. 8220.9).

Preparation of Quadruple Helices (Annealing)

G-quadruplexes types **I**, **II**, **III,** and **IV** were formed by dissolving L**1**-**4** and S**1**-**4** in the appropriate phosphate buffer and annealed by heating to 90°C for 20 min followed by slow cooling to room temperature. The solutions were equilibrated at 25°C for 24 h before performing the experiments.

Native Gel Electrophoresis

Native gel electrophoreses were run on 20% non-denaturing polyacrylamide gels in 1× TB buffer, pH 7.0 with 40 m*M* NaCl (or KCl). The TEL-ODNs were dissolved in 0.1 m*M* EDTA, 10 m*M* NaH_2PO_4, 30 m*M* NaCl (40 m*M* Na^+ buffer), or 0.1 m*M* EDTA, 10 m*M* NaH_2PO_4, 70 m*M* NaCl (80 m*M* Na^+ buffer) at a quadruplex concentration of 400 μM or 10 μM and annealed as described earlier. Samples were loaded at a final concentration of 200 μM TEL-ODNs in the buffer solution containing 6% glycerol that was added just before gel loading. The gels were run at room temperature at constant voltage (100 V) for 2.5 h. The bands were visualized by UV shadowing and after "stain all" coloration.

CD Experiments

The ODNs were prepared at a quadruplex concentration of 1.0×10^{-5} M in the appropriate buffer. Spectra were collected over a wavelength range of 200–320 nm with a scanning speed of 100 nm/min, a response time of 16 s, a bandwidth of 2.0 nm at 25°C. A background scan of buffer alone was subtracted from all scans. CD thermal denaturation experiments were followed by recording the CD values at 264 nm in a temperature range of 25–90°C at a heating rate of 0.5°C/min.

^{1}H NMR Experiments

1D NMR spectra were acquired as 16384 data points with a recycle delay of 1.0 s at temperatures of 25, 45, 65, and 85°C. Data sets were zero filled to 32,768 points before Fourier transformation and apodized with a shifted sinebell squared window function. Pulsed-field gradient DPFGSE[32,33] sequence was used for H_2O suppression. All NMR samples were prepared at 0.5 m*M* quadruplex concentration in H_2O/D_2O (9:1, v/v) in 10 m*M* KH_2PO_4, 0.2 m*M* potassium EDTA, and 70 m*M* KCl (K^+ buffer) and 10 m*M* NaH_2PO_4, 0.2 m*M* sodium EDTA or 70 m*M* NaCl (Na^+ buffer).

Molecular Modeling

The conformational features of the TEL-ODNs S**1**-**4** have been explored by means of a molecular modeling study. All the calculations were performed on a personal computer running the HyperChem 7.5 suite of programs. The AMBER force field using AMBER 99 parameter set was used.[34] The initial coordinates for the starting model of $[d(TGGGGT)]_4$ G-quadruplex were taken from the NMR solution structure of the $[d(TTGGGGT)]_4$ G-quadruplex (Protein Data Bank entry number 139D), choosing randomly one of the four available structures. The initial $[d(TGGGGT)]_4$ G-quadruplex model was built by deletion of the 5′-end thymidine residue in each of the four TTGGGGT strands. The complete structures of S**1**-**4** were then built using the HyperChem 7.5 building tool. Partial charges for each atom of the TEL were assigned using the Gasteiger-Marsili algorithm[35] implemented in the QSAR module of HyperChem suite. The resulting coordinates of the TEL atoms were energy-minimized in vacuum keeping all DNA coordinates frozen (500 cycles of the steepest descent method). The calculations were performed using a distance-dependent macroscopic dielectric constant of 4*r*, and an infinite cut-off for nonbonded interactions to partially compensate for the lack of solvent used. Hydrogen bond and glycosidic torsion angle constraints were used according to NMR and CD data. Upper and lower distance limits of 2.0 Å and 1.7 Å for hydrogen-acceptor distance, and 3.0 Å and 2.7 Å for donor–acceptor distance were used (20 kcal/mol $Å^2$). Glycosidic torsion angles were constrained to a range of $-160°/-70°$ as required for a parallel G-quadruplex having all guanines in the anti orientation (16 Kcal/mol $Å^2$). In each case, the entire system was energy minimized using the conjugate gradient method until convergence to an rms gradient of 0.1 kcal/mol Å was reached. In the next step the coordinates of all the thymidines and TEL atoms where subjected to a restrained molecular dynamics (MD) simulation. The system was initially heated from 0 to 1000 K during the first 33 ps of simulation, the simulation then proceeded for 250 ps at 1000 K and was followed by 24 ps of cooling to 273 K. Finally, all the restraints were removed and the systems were energy minimized using 1000 cycles of the steepest descent method followed by the conjugate gradient method until convergence to a rms gradient of 0.1 kcal/mol Å.

The authors are grateful to Dr. Nichola Garbett and Professor Jonathan B. Chaires, James Graham Brown Cancer Center, University of Louisville (US), for their discussions and suggestions and Dr. Luisa Cuorvo for the technical assistance. The "Centro di Servizi Interdipartimentale di Analisi Strumentale", CSIAS, is acknowledged for supplying the NMR facilities.

REFERENCES

1. Parkinson, G. N. Quadruplex Nucleic Acids; RSC Publishing: London, 2006; Chapter 1.
2. Patel, D. J.; Phan, A. T.; Kuryavyi, V. Nucleic Acids Res 2007, 35, 7429–7455.
3. Riou, J.-F.; Gomez, D.; Morjani, H.; Trentesaux, C. Quadruplex Nucleic Acids; RSC Publishing: London, 2006; Chapter 6.
4. Dexheimer, T. S.; Fry, M.; Hurley, L. H. Quadruplex Nucleic Acids; RSC Publishing: London, 2006; Chapter 7.
5. Huppert, J. Quadruplex Nucleic Acids; RSC Publishing: London, 2006; Chapter 8.
6. Pileur, F.; Andreola, M. L.; Dausse, E.; Michel, J.; Moreau, S.; Yamada, H.; Gaidamarov, S. A.; Crouch, R. J.; Toulmé, J. J.; Cazenave, C. Nucleic Acids Res 2003, 31, 5776–5788.

7. Wang, K. Y.; McCurdy, S.; Shea, R. J.; Swaminathan, S.; Bolton, P. H. Biochemistry 1993, 32, 1899–1904.
8. Chou, S.-H.; Chin, K.-H.; Wang, A. H.-J. Trends Biochem Sci 2005, 30, 231–234.
9. Levesque, D.; Beaudoin, J.-D.; Roy, S.; Perreault, J.-P. Biochem J 2007, 403, 129–138.
10. Girvan, A. C.; Teng, Y.; Casson, L. K.; Thomas, S. D.; Jueliger, S.; Ball, M. W.; Klein, J. B.; Pierce, W. M., Jr.; Barve, S. S.; Bates, P. J. Mol Cancer Ther 2006, 5, 1790–1799.
11. Phan, A. T.; Kuryavyi, V.; Luu, K. N.; Patel, D. J. Quadruplex Nucleic Acids; RSC Publishing: London, 2006; Chapter 3.
12. Bhavesh, N. S.; Patel, P. K.; Karthikeyan, S.; Hosur, R. V. Biochem Biophys Res Comm 2004, 317, 625–633; and references cited therein.
13. Oliviero, G.; Amato, J.; Borbone, N.; Galeone, A.; Varra, M.; Piccialli, G.; Mayol, L. Biopolymers 2006, 81, 194–201 and references cited therein.
14. Searle, M. S.; Williams, H. E. L.; Gallagher, C. T.; Grant, R. J.; Stevens, M. F. G. Org Biomol Chem 2004, 2, 810–812 and references cited therein.
15. Chen, J.; Zhang, R. L.; Min, J. M.; Zhang, L. H. Nucleic Acids Res 2002, 30, 3005–3014.
16. Virgilio, A.; Esposito, V.; Randazzo, A.; Mayol, L.; Galeone, A. Bioorg Med Chem 2005, 13, 1037–1044.
17. Risitano, A.; Fox, K. R. Nucleic Acids Res 2004, 32, 2598–2606.
18. Rachwal, P. A.; Findlow, I. S.; Werner, J. M.; Brown, T.; Fox, K. R. Nucleic Acids Res 2007, 35, 4214–4222.
19. Rachwal, P. A.; Brown, T.; Fox, K. R. FEBS Lett 2007, 581, 1657–1660.
20. Bugaut, A.; Balasubramanian, S. Biochemistry 2008, 47, 689–697.
21. Oliviero, G.; Borbone, N.; Galeone, A.; Varra, M.; Piccialli, G.; Mayol, L. Tetrahedron Lett 2004, 45, 4869–4872.
22. Oliviero, G.; Amato, J.; Borbone, N.; Galeone, A.; Petraccone, L.; Varra, M.; Piccialli, G.; Mayol, L. Bioconjugate Chem 2006, 17, 889–898.
23. Petraccone, L.; Erra, E.; Esposito, V.; Randazzo, A.; Mayol, L.; Nasti, L.; Barone, G.; Giancola, C. Biochemistry 2004, 43, 4877–4884.
24. Jin, R.; Gaffney, B. L.; Wang, C.; Jones, R. A.; Breslauer, K. J. Proc Natl Acad Sci USA 1992, 89, 8832–8836.
25. Dapic, V.; Abdomerovic, V.; Marrington, R.; Pederby, J.; Rodger, A.; Trent, J. O.; Bates, P. J. Nucleic Acids Res 2003, 31, 2097–2170.
26. Hardin, C. C.; Perry, A. G.; White, K. Biopolymers 2001, 56, 147–194.
27. Rankin, S.; Reszka, A. P.; Huppert, J.; Zloh, M.; Parkinson, G. N.; Todd, A. K.; Ladame, S.; Balasubramanian, S.; Neidle, S. J Am Chem Soc 2005, 127, 10584–10589.
28. Jing, N.; Rando, R. F.; Pommier, Y.; Hogan, M. E. Biochemistry 1997, 36, 12498–12505.
29. Feigon, J.; Koshlap, K. M.; Smith, F. W. Methods Enzymol 1995, 261, 225–255.
30. Feigon, J. Encyclopedia of Nuclear Magnetic Resonance; Wiley: Chichester, 1996; pp 1726–1731.
31. Breslauer, K. J.; Frank, R.; Blocker, H.; Marky, L. A. Proc Natl Acad Sci USA 1986, 83, 3746–3750.
32. Hwang, T. L.; Shaka, A. J. J Magn Res 1995, A112, 275–279.
33. Dalvit, C. J. Biomol NMR 1998, 11, 437–444.
34. Cornell, W. D.; Cieplack, P.; Bayly, C. I.; Gould, I. R.; Merz, K. M.; Ferguson, D. M.; Spellmeyer, D. C.; Fox, T.; Caldwell, J. W.; Kollman, P. A. J Am Chem Soc 1995, 117, 5179–5197.
35. Gasteiger, J.; Marsili, M. Tetrahedron 1980, 36, 3219–3228.

Reviewing Editor: Kenneth Breslauer